JOURNAL OF COMPUTATIONAL PHYSICS 23, 219–241 (1977)

Guiding-Center Simulation of Toroidal Plasmas*

THOMAS H. JOHNSON AND JOHN KILLEEN

University of California, Lawrence Livermore Laboratory, Livermore, California 94550, and Department of Applied Science, Davis, California 95616

OSCAR A. ANDERSON AND MARVIN E. RENSINK

University of California, Lawrence Livermore Laboratory, Livermore, California 94550

Received October 16, 1975; revised July 1, 1976

A new computer simulation method for axisymmetric toroidal plasmas is developed. The method comprises two separate physical models representing different components of an experimental plasma. The first model is an MHD fluid equilibrium representation; the technique devised for the solution of this equilibrium is faster than any currently in common use. The second model is a macroparticle representation which uses guiding-center formalism for the particles' velocities and positions; consequently, the timestep used by this model may be many times longer than those possible for conventional macroparticle simulations. A new computer code, GUIDON, which incorporates in these models a solution for self-consistent magnetic fields, is presented. Special features of the guiding-center model are discussed in detail. Results of simulations using GUIDON are also presented.

INTRODUCTION

Most numerical models used in the study of high-temperature plasmas have heretofore fallen into two distinct classes: fluid and particle simulation models. Fluid models deal with sets of equations, such as the magnetohydrodynamic (MHD) equations, defining the macroscopic properties of the plasma—pressure, temperature, and density—as functions of time and space, including external forces and the evolution of magnetic fields affected by the plasma motion. Particle simulation models attempt to represent the microscopic processes of the plasma more accurately, by assigning a representative charge and mass to each of a large number of macroparticles, then allowing each to evolve in time and space according to proper (Newtonian or relativistic) equations of motion. Usually some components of electromagnetic fields are computed self-consistently for this motion.

* Work performed under the auspices of the U.S. Energy Research and Development Administration.

ISSN 0021-9991

Fluid models have the advantages of considering problems involving large and complex geometries, of producing results which may easily be correlated with experimental data, and of simulating phenomena which occur over relatively large time and length scales. Particle simulation permits the study of extremely fast processes and the investigation of complex interactive processes on very short length scales.

Unfortunately, these advantages are to a large extent mutually exclusive, and an advantage in one method appears as a lack, and hence a disadvantage, in the other. In the work to be described here, an attempt has been made to create a model which combines certain of the advantages of both existing classes. Specifically, the method sought would be able to deal with problems both large and complex in configuration space and occupying times at least in the intermediate range (many hundreds of gyroperiods, if not many milliseconds) while at the same time permitting some detailed study of microscopic motions of the plasma and local development of its dominant self-consistent fields.

Particle simulation methods in common use operate under severe restrictions on timestep, problem size, and number of particles. Typically, the physical dimensions of the plasma to be simulated must be quite small (usually considered part of an infinite plasma), and the total physical time simulated quite short; statistical requirements on the calculation of fields dictate large numbers of particles. The technique presented in this paper allows all three of the above restrictions to be relaxed. It is applicable to many experimental devices of current interest.

The essence of this technique is the substitution of the guiding-center equations of motion for a more direct Newton–Lorentz force equation in advancing the velocities and positions of the particle in time. The guiding-center equations arise from the fact that, if certain conditions are met, fast gyromotion of charged particles around magnetic field lines can be averaged out, leaving just the motion parallel to the field lines and the slow drift motion in the perpendicular direction. The trajectories defined by the guiding-center equations are not those of the individual ions or electrons, but of the centers of their circular gyro-orbits. Thus these points (the guiding centers), and not the actual physical particles, are the simulation particles used in the model; the details of gyromotion are not followed. Where stability of integration might require a particle model to execute between 5 and 30 timesteps in traversing a single gyro-orbit–even though the orbit itself were of no particular significance—the guiding-center equations may take timesteps as long as several gyroperiods.

The problem of computation of MHD equilibrium configurations in toroidal geometries has received considerable attention [1–4]; the methods currently in use satisfy physical and computational criteria of convergence and accuracy. However, all these methods were designed to consider only the equilibrium solution itself. Because the computation required was not inherently long, it was not necessary to search for ways to achieve large savings in running time and efficiency. But if one intends to use such an equilibrium calculation as part of a more general numerical algorithm, and particularly if it is to be repeated as one step of a cyclic process, existing methods may take too long to be practical. A self-consistent solution of the

magnetic fields generated by the macroparticles and by the fluid required a very rapid solution to Ampere's law to alternate with cycles in which the macroparticles moved.

Cylindrical coordinates are used in this solution, and axial symmetry is assumed so the calculational domain is (r, z), as shown in Fig. 1. The parameters used to illustrate the method will be those of a Tokamak, though other appropriate devices would serve as well.

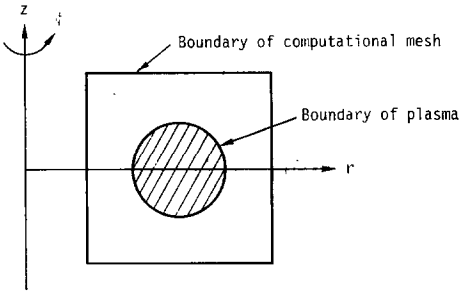

FIG. 1. Calculational domain for cylindrical coordinates.

The computation of magnetic surfaces in the Two-Energy Component Toroidal Fusion Test Reactor (TFTR) is presented as an application of the GUIDON code.

TOROIDAL MHD EQUILIBRIUM

We consider hydromagnetic equilibria for a toroidal plasma with a scalar pressure. The basic equations are

$$\nabla p = (1/c)\mathbf{j} \times \mathbf{B}, \tag{1}$$

$$\nabla \times \mathbf{B} = (4\pi/c)\mathbf{j}, \tag{2}$$

$$\nabla \cdot \mathbf{B} = 0. \tag{3}$$

We assume that the system is axially symmetric, and consider only the toroidal component, j_ϕ, of the current density. The poloidal flux function $\psi(r, z)$ is then given by

$$-\frac{1}{r}\frac{\partial^2\psi}{\partial z^2} - \frac{\partial}{\partial r}\left(\frac{1}{r}\frac{\partial\psi}{\partial r}\right) = \frac{4\pi}{c} j_\phi, \tag{4}$$

where

$$B_r = -\frac{1}{r}\frac{\partial\psi}{\partial z} \qquad B_z = \frac{1}{r}\frac{\partial\psi}{\partial r}. \tag{5}$$

Grad [5] has given the form of the right-hand side of Eq. (4) for the scalar pressure case as

$$j_\phi = c\left[rp'(\psi) + \frac{g'(\psi)}{4\pi r}\right], \tag{6}$$

where $p(\psi)$, the scalar pressure, and

$$g(\psi) = \tfrac{1}{2}r^2B_\phi^2 \tag{7}$$

are given functions of ψ, and B_ϕ is the toroidal component of the magnetic field. We shall set

$$g'(\psi) = f(\psi)\,f'(\psi), \tag{8}$$

where

$$f(\psi) = rB_\phi = k/\nu(\psi), \tag{9}$$

with

$$\nu(\psi) = 1 + bp(\psi), \tag{10}$$

where $k = I_z/5$, with I_z in amperes, and b a given constant. (If $b = 0$, then the toroidal field reduces to the vacuum $B_\phi = I_z/5r$.)

In general, we shall want to be able to consider devices which have a vacuum poloidal field in addition to the poloidal field caused by plasma currents. It is convenient when considering Eq. (4) to let

$$\psi = \psi_c + \psi_p\,, \tag{11}$$

where ψ_c is the poloidal flux function of the vacuum magnetic field and is a known solution to

$$-\frac{1}{r}\frac{\partial^2\psi_c}{\partial z^2} - \frac{\partial}{\partial r}\left(\frac{1}{r}\frac{\partial\psi_c}{\partial r}\right) = 0. \tag{12}$$

Combining Eqs. (4), (6), and (12), we obtain

$$-\frac{\partial^2\psi_p}{\partial z^2} - r\frac{\partial}{\partial r}\left(\frac{1}{r}\frac{\partial\psi_p}{\partial r}\right) = \frac{4\pi}{c}\left[r^2p'(\psi)\right] + g'(\psi), \tag{13}$$

which is the equation for ψ_p, which we solve numerically by the method described later in this paper. We note that the left-hand side of Eq. (13) is linear in ψ_p, but the right-hand side depends nonlinearly, in general, on the total ψ. The boundary conditions used in solving Eq. (13) are those appropriate to the plasma fields only.

The choice of the functional dependence of p on ψ is arbitrary, but a choice which can be adjusted to fit many experimentally observed pressure profiles is

$$p(\psi) = \bar{c}(\psi - \psi_0)^m, \qquad \text{for} \quad \psi \geqslant \psi_0,$$
$$= 0, \qquad \text{elsewhere,}$$

where $\bar{c}$ and m are given constants and ψ_0 is a reference flux surface defining the boundary of the plasma.

Guiding-Center Particle Model

Since simulation of high-energy electron currents is one of the proposed uses of this method, all particle equations of motion are relativistic.

Application of the guiding-center equations assumes invariance of the magnetic moment, μ, of the particles [6],

$$\mu = \gamma^2 m_0 v_G^2/(2B), \tag{14}$$

where m_0 is the particle's rest mass, B is the magnetic field, $B = |\mathbf{B}|$, $\gamma = (1 - v^2/c^2)^{-1/2}$, and v_G is the gyrovelocity. The validity of this assumption requires that changes in B seen by the particle be very small during the course of a gyro-orbit.

The geometry is two-dimensional, cylindrical, and axisymmetric, as illustrated in Fig. 1. ϕ is the symmetry coordinate, and it is assumed that motion is identical in each $r - z$ planar cross section of the torus. However, all three components of the magnetic field are calculated at each point in the 2-D computational domain, and all three components of both position and velocity are calculated for each particle. For this reason the code falls into a category known in the vernacular as "2½-dimensional." The particles are actually treated as rings of charge going around the torus, but their true three-dimensional location must be known to locate their turning points, as in trapped particle orbits.

The model described in this paper neglects self-consistent electrostatic interactions. (Results without this limitation will be given in a future publication.) The assumption is that the plasma is both macroscopically and microscopically neutral. In the former case, this amounts to assuming a uniform neutralizing background of particles of charge opposite to the simulation particles; in the latter case, the model assumes that the energy density in electrostatic interactions is far less than the local energy density in magnetic fields. Clearly very strong magnetic fields are required.

Finally, the model assumes that the total energy of each particle is conserved; thus radiative and collisional processes are ignored. A key feature of many devices is an applied toroidal electric field used to accelerate the plasma current. This field is supplied inductively by the rapidly changing flux of an additional vacuum coil with

time-dependent current; the plasma may then be seen as the secondary winding of a transformer. The details of this process are not treated; the model merely assumes that a curl-free electric field exists within the torus. The correct terms for electric drift are included in the guiding-center equations, and kinetic energy is supplied to (or removed from) the particles by the electric field at each timestep, according to $\Delta W^n = -\left(qr\frac{V}{2\pi}\right)\Delta\phi^n$, where $\Delta\phi^n$ is the toroidal angle the particle has moved through from time $(n-1)$ to time n, and $V/2\pi r$ is the electric field. The toroidal component of electric field induced by changing the plasma current has been allowed for in some coded versions of the model.

At each timestep, then, the following quantities are known for each particle: position in three dimensions, kinetic energy, and magnetic moment. The values of all components of **B** at the particle's position can be found by interpolation from a mesh of values; a straightforward bilinear interpolation is used. The particle's gyrovelocity may then be computed from Eq. (14). Conservation of energy is then invoked to determine $v_\parallel$, the velocity parallel to the magnetic field. By definition,

$$\gamma \equiv \left(1 - \frac{v^2}{c^2}\right)^{-1/2} \approx \left(1 - \frac{v_\parallel{}^2 + v_G{}^2}{c^2}\right)^{-1/2} \tag{15}$$

(the drift velocity v_D has been neglected because of the basic assumption $v_D \ll v_G$); then solving for $v_\parallel{}^2$,

$$v_\parallel{}^2 = c^2[1 - (1/\gamma^2)] - v_G{}^2. \tag{16}$$

The form of Eq. (16) is useful, since it may be used to check for the particle's arrival at a mirror point (the end of a banana). As the particle passes through a mirror point in the course of one timestep, $v_\parallel{}^2$ in (16) will go negative, indicating that the particle has entered a region forbidden by its laws of motion. It will not have entered very far, however, for as $v_\parallel \to 0$, the error incurred by not turning the particle *exactly* at its mirror point will be very small (the single-particle orbit code by Anderson and Fuss [7] from which the guiding-center formulation was adopted conserved the longitudinal adiabatic invariant J to better than 1 part in 10^6 over orbits including many bounces). Mirroring is very simply accomplished by keeping track of the sign of $v_\parallel$ for every particle (the sign is stored conveniently as the sign of μ, which we know to be positive definite; it is thus easy to spot trapped particles in output listings by watching the sign of μ). When $v_\parallel{}^2$ is calculated as being negative, the signs of $v_\parallel$ and μ are changed.

Using the resulting $v_\parallel$ and appropriate derivatives of **B** at the particle's position, the drift velocity $\mathbf{v}_D$ of the guiding center (due to all three sources) is calculated using

$$\mathbf{v}_D = \frac{\mathbf{b}}{B} \times \left(c\mathbf{E} + \frac{\mu c}{\gamma e}\nabla B\right) + \frac{c\gamma m_0 v_\parallel{}^2}{eB}[\mathbf{b} \times (\mathbf{b}\cdot\nabla)\,\mathbf{b}]; \tag{17}$$

$\mathbf{b} \equiv \mathbf{B}/B$ and $B \equiv |\,\mathbf{B}\,|$. The term-by-term form of (17) actually used in the running

code is shown in the Appendix for the reader's convenience. The total velocity of the guiding center may now be calculated as the sum

$$\mathbf{v} = \mathbf{v}_{\parallel} + \mathbf{v}_{\mathrm{D}} . \tag{18}$$

Henceforward we shall call this the particle's velocity, since the particles represented by the code are actually guiding centers.

We may now update the particle's position from time n to $n + 1$. This update is accomplished by a "leapfrog-corrector" technique, in which a trial value at $n + 1$ is generated by a standard leapfrog difference procedure; using that new position and local fields, Eqs. (16)–(18) are used to find a trial value of v^{n+1}. All of this is done to provide an approximate value of $v^{n+1/2}$, thus properly time centering the equation $dx/dt = v$; a simple difference $(x^{n+1} - x^n)/\Delta t = v^{n+1/2}$ may then be used, and v^{n+1} may be evaluated at the new position. If $\mathbf{x}$ is the general position vector, the four-step procedure is:

Step 1. $(\mathbf{x}^{n+1})^* = \mathbf{x}^{n-1} + 2\Delta t V^n$.

Step 2. $(\mathbf{x}^{n+1})^* \rightarrow$ [guiding-center formalism] $\rightarrow (\mathbf{v}^{n+1})^*$.

Step 3. $\mathbf{x}^{n+1} = \mathbf{x}^n + (\Delta t/2)[\mathbf{v}^n + (\mathbf{v}^{n+1})^*]$.

Step 4. $\mathbf{x}^{n+1} \rightarrow$ [guiding-center formalism] $\rightarrow \mathbf{v}^{n+1}$.

With the particles at new positions at time $n + 1$, it is now necessary to solve for new values of the self-consistent fields over the whole computational mesh, after which the above process is repeated.

The solution for self-consistent fields relies on a quasi-static approximation; the fields are found at each timestep from Ampere's law, Eq. (2). A further approximation is that only the toroidal components of current are considered, thus only the toroidal component of particle velocity is used in constructing the source terms $\mathbf{j}$ for Eq. (2). Like the earlier assumption that magnetic interactions dominate electric ones, this assumption limits applicability of the method and must be kept in mind when applying it. Both were chosen because they greatly simplify the computational problem, and because they can reasonably be applied to certain phases of most axisymmetric toroidal devices.

Although the simulation particles are moved about as though each is a single deuteron or electron, each particle actually represents many real particles distributed uniformly in a ring around the symmetry axis of the torus. Thus, the local current density, in statamperes per square centimeter, represented by a single simulation particle is defined as

$$J_\phi = \frac{eNv_\phi}{2\pi r\, \Delta r\, \Delta z}, \tag{19}$$

where N is the total number of deuterons or electrons per simulation particle.

Writing the toroidal velocity as $v_\phi = r(d\phi/dt)$, the current density per simulation particle becomes

$$J_\phi = \left(\frac{eN}{2\pi\, \Delta r\, \Delta z}\right) \frac{d\phi}{dt}. \tag{20}$$

The total current density of all the simulation particles is

$$j_\phi = \sum J_\phi \tag{21}$$

and is added to the rhs of Eq. (13). Currents defined by (21) are assigned spatial locations on a mesh by the common technique known as "area weighting," [8] in which fractions of the current for each particle are assigned to the four nearest mesh points in bilinear proportions. Since this can be thought of as enlarging the simulation particles from points to the size of a cell, they are known in the vernacular as "macroparticles" or super particles. In codes which calculate all self-consistent electromagnetic interactions, the sharp square edges of macroparticles obtained by area weighting are inadequate; the particles must be more smoothly shaped (as, for instance, a modified Gaussian) to prevent anomalous high-frequency components from being introduced into the radiated fields. Since our model has no radiated fields and is essentially quasi-static in nature, no such correction to the simple bilinearity of area weighting is necessary.

Special Features of the Particle Model

An advantage of using the guiding-center equations is that fewer particles are required to perform a simulation than might be required by more conventional codes. The number of particles required is dictated solely by the dynamics to be simulated—on how small a scale motions which affect the overall distribution actually occur. Typically, the number is more than an order of magnitude less than what one commonly thinks of for full-simulation codes.

Studies must be performed during each simulation to guarantee that enough particles are being used. These may most obviously (but most expensively) be accomplished by raising the number of particles and repeating runs until no differences in spatial and velocity distribution are observed after long times. Fortunately, such studies (performed for a variety of simulation problems) do not reveal a great variance in the particle requirements.

The orbit integration involves only the solution of an ordinary differential equation and thus is not subject to the customary Courant condition limiting the timestep. However, a practical timestep limitation is introduced by the relation

$$\Delta t \leqslant \hat{r}/2\hat{v}, \tag{22}$$

where $\hat{r}$ is the smallest radius of curvature involved in the guiding-center poloidal

motion and $\hat{v}$ is an averaged poloidal velocity. For larger values of Δt the straightline orbit segments of each timestep may be too long to approximate the curvature properly, and the subsequent motion will be distorted.

A more serious difficulty arises from the fact that the basic calculational cycle—solve for **B**, move particles, update currents, solve for **B**—is not properly time centered. The use of the guiding-center equations implies that a time integral has already been performed over one gyroperiod, the result being that one has no equation of motion for $d\mathbf{v}/dt$; one has merely an algebraic expression for **v** at each timestep. Proper centering would have the velocities, currents, and fields defined half a timestep displaced from the positions. However, **v**, **r**, and **B** are all calculated at even timesteps. The inconsistencies which result are apparent when one considers that both $(v^{n+1})^*$ and v^{n+1} in the leapfrog corrector algorithm are evaluated using $\mathbf{B}^n$. Clearly this imposes the requirement that both particle and field quantities do not change too much in one timestep. This restriction is most severe when strong field gradients exist, as in the case of strongly interacting particles.

The accuracy of the particle orbit integration algorithm was tested by comparing results for single-particle orbits with analytically calculable orbits in simple magnetic configurations. Results for more complex magnetic configurations were compared with the orbit code of Anderson and Fuss [7]. The accuracy was very good for timesteps typically used in applications of the code.

The interdependence of **v**, **j**, and **B** requires some care in the initialization of problems. The first step in preparing for the particles' motion (once they have been located in the vacuum field or plasma current field) is to calculate their magnetic moment. However, the resulting value of μ is not the permanently conserved quantity, because the self-consistent fields of the particle currents have not yet been taken into account in this calculation. A simple relaxation or renormalization procedure is used, in which the magnetic moment μ is recalculated for particles at fixed positions in the most recently defined **B**. Total velocities and **B** are then redefined on the basis of these μ's, and the procedure repeated. It converges quite rapidly, usually in less than three cycles.

The problem of particle sticking was the most severe difficulty encountered in the development of a workable guiding-center particle pusher. The visible manifestation of the problem was that some trapped particles spent long periods of time—even hundreds of cycles—apparently not moving in the poloidal plane, or in tracing out minute fractions of what their orbits should have been. When a particle has just mirrored, its velocity is still quite small for at least two or three, and often as many as five or six timesteps. During this otherwise uninteresting part of its orbit, the particle motion is particularly sensitive to the time-dependent part of **B**. Quite small changes in local magnetic field caused by collective effects of other particles may suddenly make it appear that the particle in question has passed a mirror point again. For example, at cycle n, particle p mirrors, changing the sign of $v_\parallel$; because of its small velocity it travels less than a cell width in Δt, moving to a point where the local $|B|$ is only 0.5% less than $|B|_{\text{mirror}}$. Between cycles n and $n+1$, with all the particles fixed, B_{poloidal} is updated and changes at the four neighboring mesh points raise $|B|$

at the location of p by 1%. At cycle $n + 1$ p will again change the sign of $v_\parallel$, heading actually toward a region of higher $|B|$. The particle will have become "stuck" in an artificially created magnetic well.

The effect is a result of the discretization of the time scale imposed by the numerical solution. In this form, it is peculiar to the guiding-center equations of motion and is essentially unavoidable.

The solution to this problem is to recalculate μ for each particle at its turning point. This results in smooth trajectories with precise turning points. This approach was avoided at first on the grounds that it meant tampering with the validity of the model, since constant μ is fundamental. But exhaustive studies of the effects of the technique show that $\Delta\mu$ is usually on the order of 0.5%, and rarely as much as 2%. Some changes in two turnings amounting to as much as 4% were observed occasionally in simulations of rather turbulent plasmas, but subsequent changes always resulted in cumulative $\Delta\mu$'s on the order of 2%.

It appears that the temporally discrete guiding-center formalism introduces artificial nonadiabaticity into a simulation, in much the same manner in which spatially discrete meshes introduce artificial diffusion into hydrodynamics codes. Approximating variables continuous in time with ones which can only behave as step functions generates unavoidable small inaccuracies. Overall effects of the $\Delta\mu$ "correction" (and, in fact, the reasonableness of the entire model) have been studied by calculating other theoretically conserved quantities. The second adiabatic invariant J,

$$J \equiv \int m\mathbf{v} \cdot \mathbf{ds} = m_0 \int \gamma v_\parallel \, ds \tag{23}$$

should be the one most drastically affected by changing μ. Though it is not conserved here to the phenomenal degree that it is in Anderson and Fuss' single-particle code [7], it does remain constant to within about 1 part in 10^4. Also, the ϕ component of the cyclotron-averaged canonical angular momentum

$$P_\phi \equiv \gamma m_0 r v_\phi + (e/c)\, r A_\phi \tag{24}$$

is an exact rather than an approximate invariant of the motion. Its conservation gives a good measure of the relative magnitude of errors introduced by $\Delta\mu$ compared to those endemic to the entire model, since passing particles have no $\Delta\mu$ correction but should also conserve $\mathbf{P}_\phi$. It was found that both trapped and passing particles conserve $\mathbf{P}_\phi$ to about 1 part in 10^6. Therefore, $\Delta\mu$-generated errors fall within the other limitations of the model.

Solution of the Magnetic Field Equation

Solution of Eq. (13) requires that the sources j be defined over the computational mesh and the appropriate boundary conditions on ψ specified. Because of the differential form of the definition of the B components, it is convenient to have the

flux values centered between field values; Eq. (13) requires that ψ and j have the same centering. Thus interlocking computational meshes are implied; e.g., for a typical field mesh 64×64, the mesh defining j and ψ is offset by $\Delta r/2$ and $\Delta z/2$.

The most convenient assumption for boundary conditions is perfectly conducting walls. We then have a Dirichlet problem; specifically, $\psi_p = 0$ on the boundaries. There are two alternate justifications for this assumption. First, the actual machine simulated may have conducting walls; however, the shape of our computational domain is rectangular, whereas conducting walls in experimental devices frequently have a circular cross section in the $r - z$ plane. Second, the computational boundaries may be removed far enough from the critical region of the problem so that the plasma equilibrium fields go to zero. This is the situation for devices such as ATC, where an externally applied vertical centering field is used to set the major radius of the plasma, and the walls do not play a significant role in the plasma equilibrium. The solution of Eq. (13) proceeds in three steps:

Step 1. Fourier transform the equation in the z direction. In the operation of the code only the source terms need be transformed at this stage. A fast Fourier transform algorithm is used; since the function is identically zero at both boundaries, only the sine transform term is necessary.

Step 2. The resulting differential equation in the r direction for each of the k modes is

$$k^2\psi_k - r\frac{\partial}{\partial r}\left(\frac{1}{r}\frac{\partial\psi_k}{\partial r}\right) = \frac{4\pi}{c} rj_k . \tag{25}$$

The equation is solved using an implicit three-point difference scheme.

Step 3. Inverse transform and normalize the ψ_k resulting from Step 2.

We actually difference Eq. (13) before transforming it, so that the leading term $k^2\psi_k$ in (25) should be replaced by a term $[(2/\Delta z)\sin(k\,\Delta z/2)]^2\,\psi_k$. Because of the use of the fast sine transform, the number of cells in the z direction must always be a power of 2. The number of cells in the r direction is not so limited, but the calculation can be made more efficient if it is an even number. With new values of ψ known, new values for B are calculated from Eq. (5), centering the differences appropriately by averaging in the direction perpendicular to the difference.

Because the source term in Eq. (13) is a function of flux, computation of the equilibrium requires a trial solution to begin. The following additional quantities make up a complete input (different quantities might be substituted if one desired a different physical definition of the problem): The total toroidal current flowing, I; the constant m in $p(\psi)$, defining the shape of the current profile; initial coordinates of the center of the plasma, (r_c, z_c) (though customarily $z_c = 0$, which will be assumed henceforth); and an estimate of the radius of the plasma, a_p.

Using these values, a trial solution is generated from the Biot–Savart law, assuming the current I is a point source at $(r_c, 0)$ with free-space boundaries. With the flux now

defined at each of the mesh points, the reference flux ψ_0 is chosen as the flux at the point (r_c, a_p). The constant $\bar{c}$ can then be evaluated by

$$\bar{c} = I \Big/ \Big[m \, \Delta r \, \Delta z \sum_{\psi \geqslant \psi_0} r(\psi - \psi_0)^{m-1} \Big]. \tag{26}$$

With all these values available the sources of Eq. (13) can be evaluated at each of the mesh points and the equation solved by the method just described. We shall refer to this solution procedure as BPHI.

At the end of this first iteration, the new ψ surfaces will differ from the Biot–Savart trial function; r_c will have changed as well, as the plasma begins to move toward its equilibrium position (call the new value r_c'). For the second iteration, it is necessary to redefine ψ_0. The new ψ_0 is chosen as ψ at (r_c', a_p). Then $\bar{c}$ is recalculated from Eq. (26), and BPHI employed once again.

This is the basic cycle of operations in one iteration: (a) redefine ψ_0; (b) recalculate $\bar{c}$; (c) use BPHI. Iteration proceeds until r_c and the flux surfaces cease to change. Once this point is reached, however, the equilibrium has not yet been found, because we have been arbitrarily limiting the radius of the plasma. So now ψ_0 is fixed and iterations are performed using only steps (b) and (c) of the cycle above, allowing the plasma to expand or contract and further adjsut r_c, if necessary.

Typically it takes between 5 and 10 complete iterations of (a)–(c), followed by only two or three of (b)–(c), to arrive at an equilibrium. The number of cycles required depends obviously on the distance from equilibrium of the trial function. Presuming one already knows the correct value of $(B_z)_{\text{vacuum}}$ (or, rather, the ψ_{vacuum} that generates it), to produce a reasonable equilibrium, the number of cycles required depends primarily on the discrepancy between initial and final values of r_c. None of the test problems run, including those where the initial position was as far as possible from equilibrium (placed at the opposite side of a doubly elongated mesh), required more than 20 iterations to reach equilibrium.

The advantage of this scheme when compared to more familiar methods of equilibrium calculation are its speed and convergence properties. A further significant advantage of this method is its generality—the ease with which it may be coupled interactively with other computation, such as macroparticle motion. After an equilibrium has been reached and the particles initialized, fluid and particle currents can easily be defined on the same mesh, and a single algorithm (BPHI) can be used to update the total flux self-consistently.

As was demonstrated by Marder and Weitzner [4], the nonlinear nature of Eq. (13) can in many situations lead not to a unique solution but to a finite number of solutions. In particular, for field problems such as this one, there tend to be two "bifurcated" solutions, a "shallow" one, in which the flux gradients are very small, and a "deep" one, in which the magnetic well is much more pronounced. Convergence, once guaranteed, may lead to the physically less desirable shallow well, depending upon the initial trial function.

The form of the source term we have chosen could be a particularly dangerous one

in this context if $\bar{c}$ is kept constant instead of I. A slight lowering of the maximum flux at any iteration without renormalization of $\bar{c}$ defined by Eq. (26) leads to disastrous consequences: The flux contained within the fixed ψ_0 being less, there is less real current in the problem; less total current will lead, on the next iteration, to a further lowering of ψ_{max}, initiating an unstable decrease. Before long (typically 10 iterations) ψ_{max} will be less than ψ_0 and the plasma current will disappear entirely. The result will have converged to $\psi = 0$ everywhere. In our model we avoid this problem by making $\bar{c}$ an implicit function of ψ via Eq. (26); i.e., we solve for ψ with fixed I rather than fixed $\bar{c}$. In this case we do not find multiple solutions.

In order to test the speed of the present algorithm it was compared with the first of the two methods proposed by Marder for finding bifurcated solutions. Their technique requires that each iteration be performed in a set of three subcycles. If, in operator notation L denotes the left-hand side of Eq. (13) and superscripts represent values of ψ at successive iterations, the method can be written:

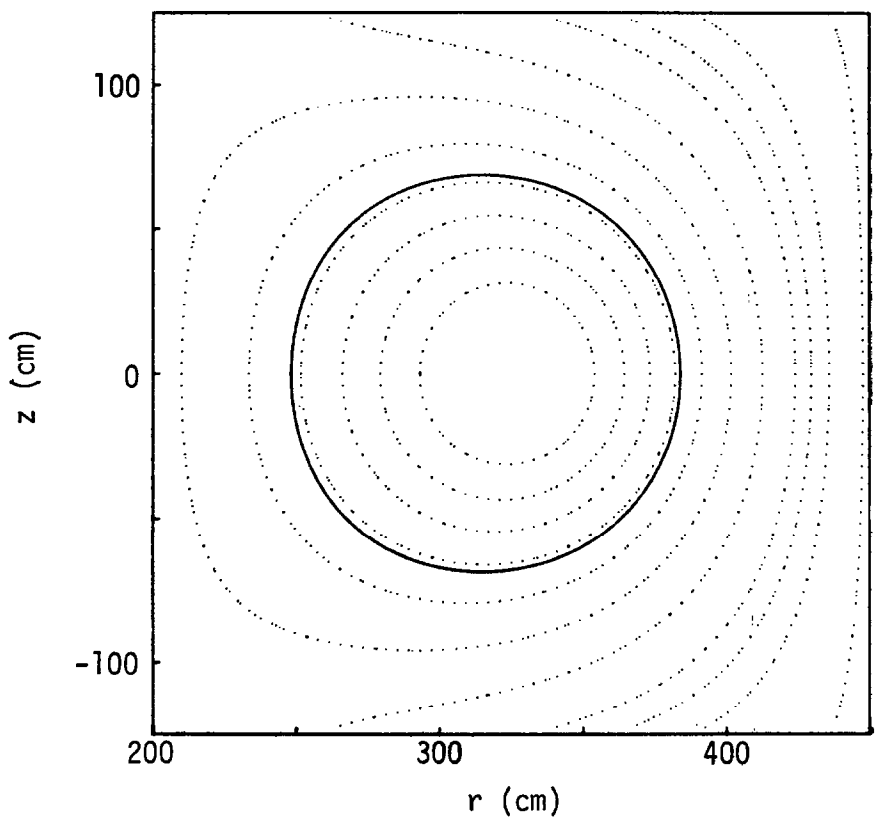

FIG. 2. Equilibrium poloidal flux contours; solid line is the plasma boundary.

(1) solve $L\psi^{n+1/3} = f(\psi^n)$;

(2) solve $L\psi^{n+2/3} = f(\psi^{n+1/3})$;

(3) calculate $\psi^{n+1} = (1 - \alpha)\,\psi^n + 2\alpha\psi^{n+1/3} - \alpha\psi^{n+2/3}$;

where α is an arbitrary constant peculiar to the problem, convergence being demonstrated for sufficiently low α. The first two steps of this method may be accomplished by a number of techniques—ADI, as in Anderson, Killeen, and Rensink [3] or the BPHI described here.

Comparisons using the Marder method with the BPHI algorithm and the procedure described earlier were run for three different cases. Equilibria produced by the two techniques were essentially identical in all cases. Since Marder's technique requires three cycles instead of one ψ^n to ψ^{n+1}, and it also requires roughly twice as many iterations $n \to n + 1$ to reach equilibrium, the present procedure is on the average almost six times faster than the Marder technique.

Callen and Dory [2] use a slightly different perfectly conducting boundary condition,

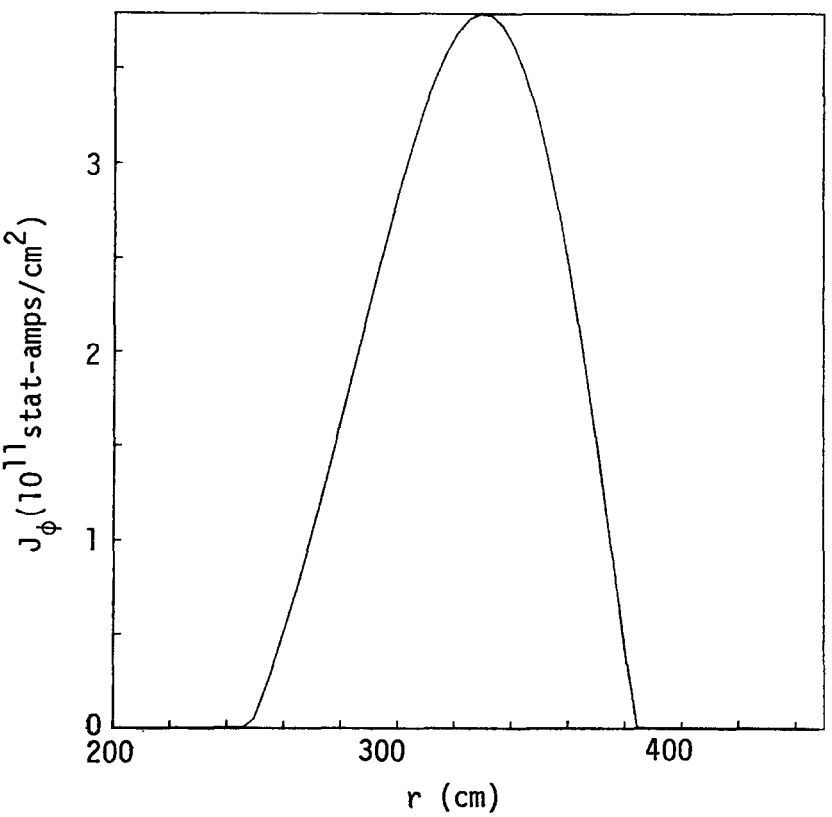

FIG. 3. Equilibrium current density along a plasma diameter.

namely, ψ = constant but not necessarily zero. To do this compatibly with their over-relaxation method of obtaining convergence, they maintain an extra artificial boundary and engage in an extrapolation procedure to readjust these boundary points and to test convergence. The boundary fluxes thus used are those generated by the trial solution. If the "bifurcation" problem is a severe one, choice of a good trial solution can force convergence to the desired physical result when this procedure is employed.

Another motivation for choosing boundary conditions in which $\psi \neq 0$ is the attempt to simulate free-space, rather than perfectly conducting, boundary conditions. This may be done by redefining the boundary fluxes at each timestep using a Biot–Savart solution (as is done here for the trial function) applied to the whole plasma current.

Both of these nonzero boundary conditions have been used successfully in conjunction with the algorithm BPHI. It was found that the simplest method was merely

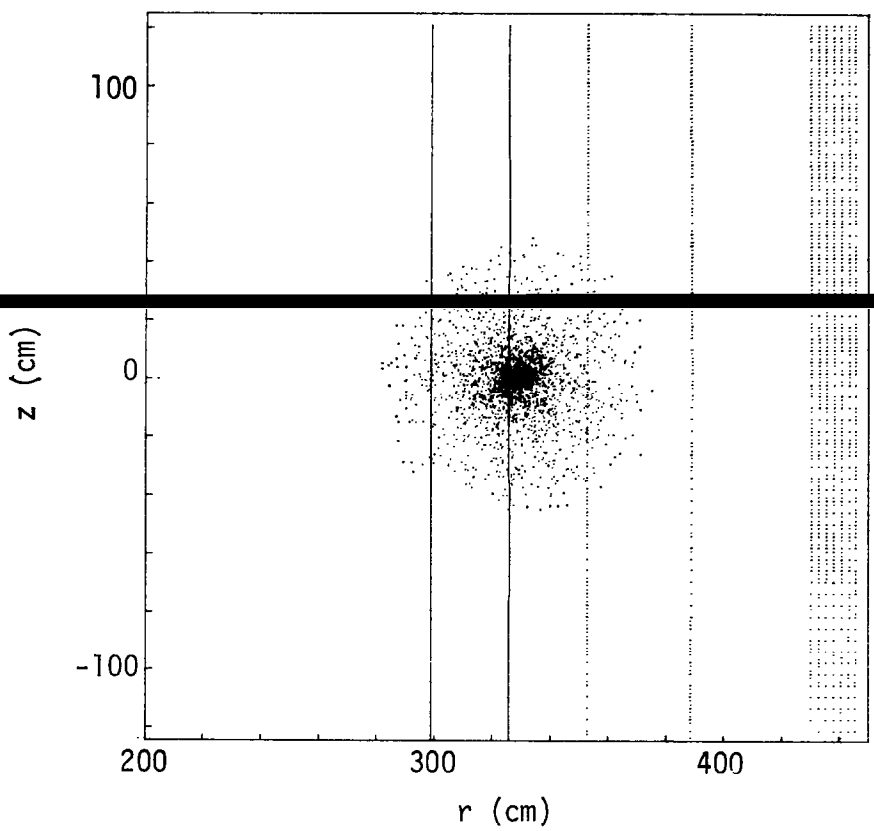

FIG. 4. Initial configuration of macroparticles in poloidal plane; the vertical lines are mod-B contours.

to set the ψ's on the boundary equal to the ψ's at the nearest inside mesh points at each cycle of BPHI (then fix them during any succeeding calculation of equilibrium changing under the influence of particle motion). Results of equilibria calculated in this manner agreed with those calculated using identical inputs, but $\psi = 0$ on the boundaries by 1 part in 10^6 at all mesh points. The method requires, of course, more coding and slightly longer running times for equilibria than does $\psi = 0$; it was therefore abandoned when it was discovered that renormalization of $\bar{c}$ (required by both kinds of boundary conditions) was by itself sufficient to force convergence to the physically desired equilibrium with the Biot–Savart trial functions.

The free-space boundary condition approximation was implemented and shown to work but has not been used extensively because one of the perfectly conducting/finite-wall assumptions was always found to be sufficient as a model for the devices studied, and use of the free-space approximation greatly increases running time of the equilibrium calculation.

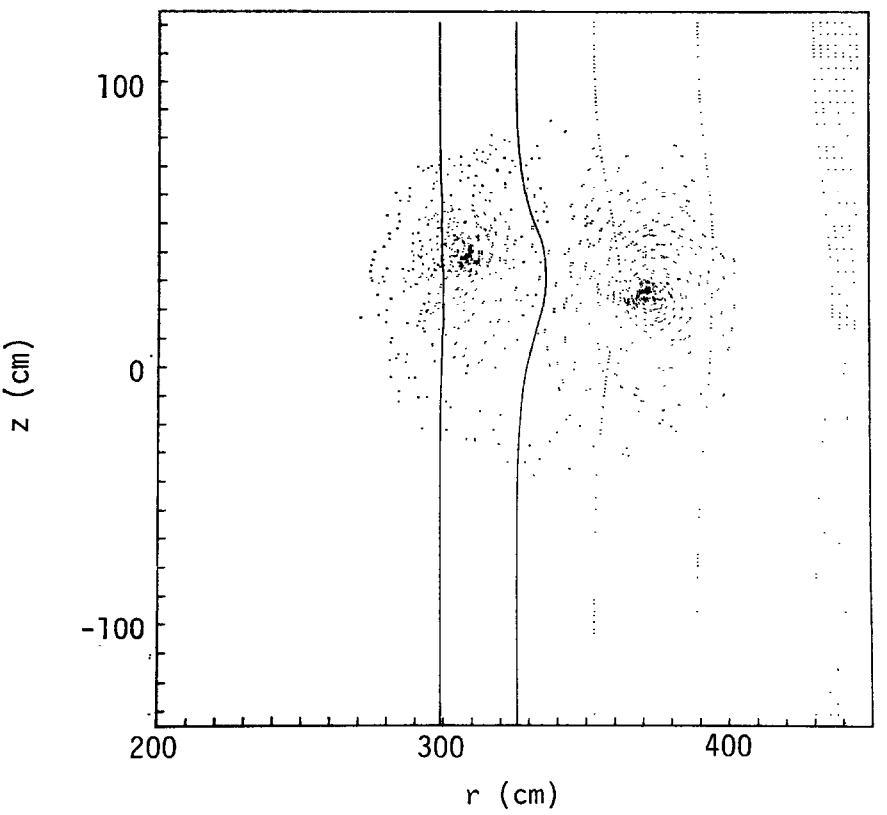

FIG. 5. Particle configuration after 18 μsec for co- and counterinjection with $\tau_{inj} = 25$ μsec.

APPLICATION

This code has been used to study the effects of injecting energetic neutral beams into a Tokamak equilibrium plasma. The beams, represented by the guiding-center model in our code, may be used primarily for heating the bulk plasma or they may directly produce fusion reactions, as in the two-component reactor concept [9].

In the application described here the Tokamak plasma is represented by the quasi-equilibrium MHD model in which the scalar pressure is given by $p(\psi) = \bar{c}(\psi - \psi_0)^2$, $\psi_0 \leqslant \psi$, where $\psi(r, z, t)$ is the poloidal flux function, ψ_0 defines the plasma boundary, and $\bar{c}$ is a constant. The toroidal plasma current density,

$$j_\phi{}^p = crp'(\psi),$$

is added to the guiding-center beam current density (21) to generate the net poloidal field from Eq. (13). The value of the constant $\bar{c}$ is adjusted during beam buildup so

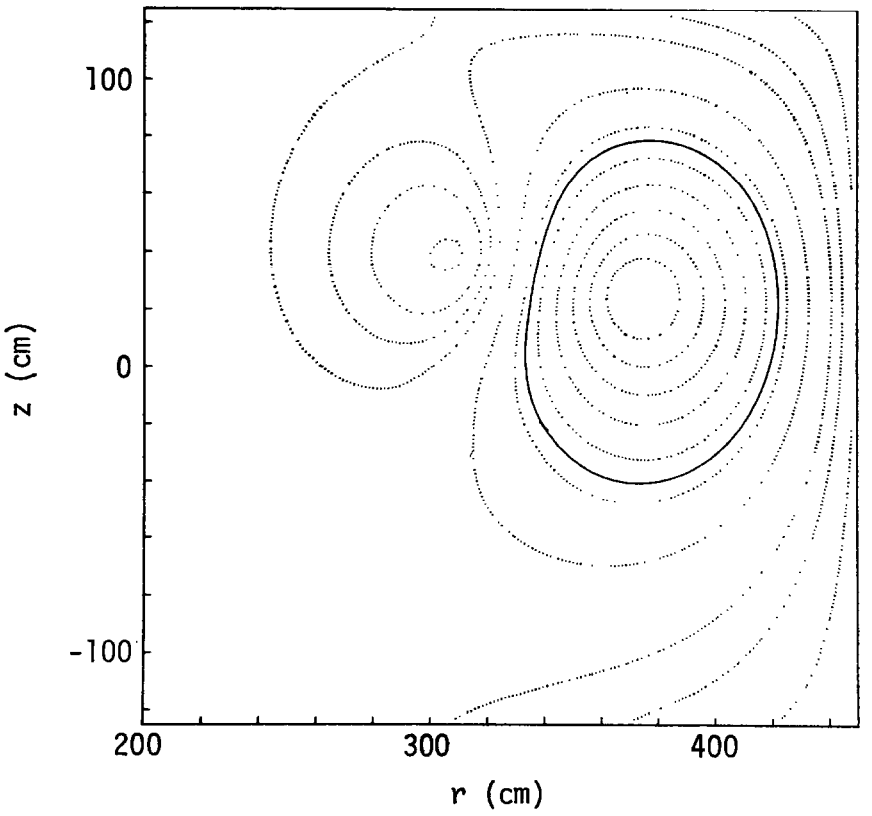

FIG. 6. Poloidal flux surfaces after 18 μsec for co- and counterinjection with $\tau_{\text{inj}} = 25$ μsec.

as to yield a fixed value for the total plasma current. Typical equilibrium plasma and magnetic field parameters are:

(plasma major radius)	$R_0 = 325$ cm;
(plasma minor radius)	$a_p = 65$ cm;
(total plasma current)	$I_T = 0.77$ MA;
(applied toroidal field)	$B_T = 37.5$ kG at $r = R_0$;
(applied vertical field)	$B_V = 425$ G.

In the absence of injected beams, poloidal flux contours are as shown in Fig. 2, and the current density profile along a plasma diameter in Fig. 3.

The guiding-center beam particles are loaded into the system with a density profile,

$$n_b(r, z) = \frac{N_b}{\pi a_b}\left(\frac{1}{\rho} - \frac{1}{a_b}\right), \tag{27}$$

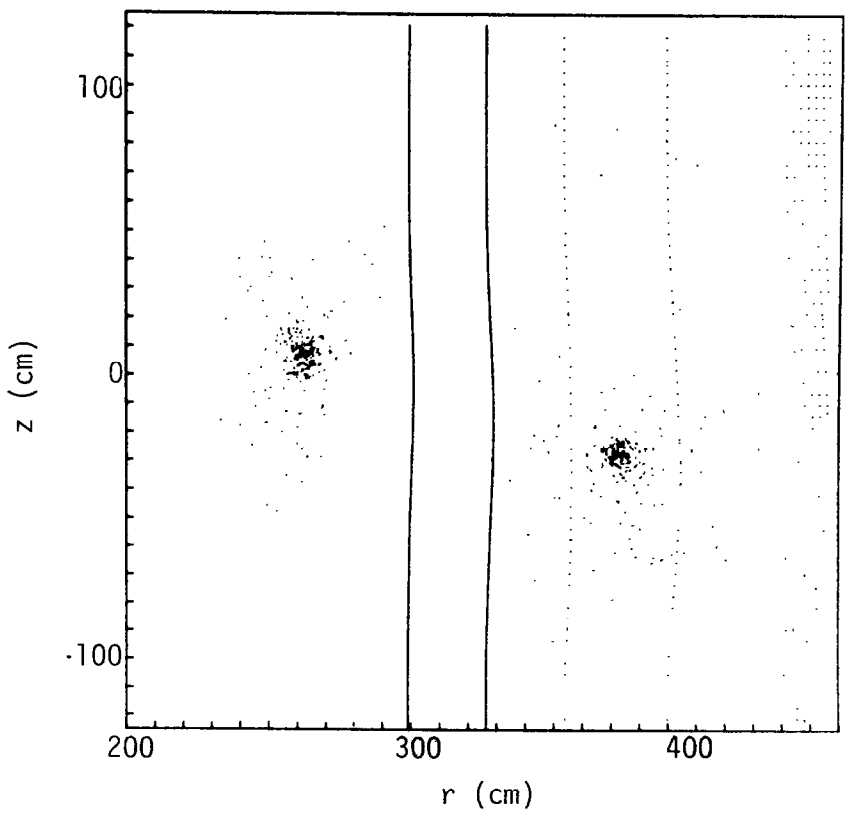

FIG. 7. Particle configuration after 75 μsec for co- and counterinjection with $\tau_{Inj} = 150$ μsec.

where

$$\rho^2 = (r - R_0)^2 + z^2 \leqslant a_b^2, \tag{28}$$

where $N_b = 2500$ is the total number of macroparticles used, and a_b is the beam deposition radius. The initial velocities of the particles are chosen to be either parallel or antiparallel to the symmetry direction, so as to represent co- and counterinjection. At the initial time, $t = 0$, all 2500 macroparticles are simultaneously loaded into the system, but the charge per macroparticle is initially zero and increases linearly in time over some finite time interval in order to represent the finite pulse duration in an actual neutral beam injection experiment. Typical beam parameters are:

(neutral beam current)	$I_b = 80$ A;
(beam pulse duration)	$\tau_b = 30$ msec;
(deuteron beam energy)	$E_b = 80$ keV;
(beam deposition radius)	$a_b = 50$ cm;

and the initial particle positions are shown in Fig. 4.

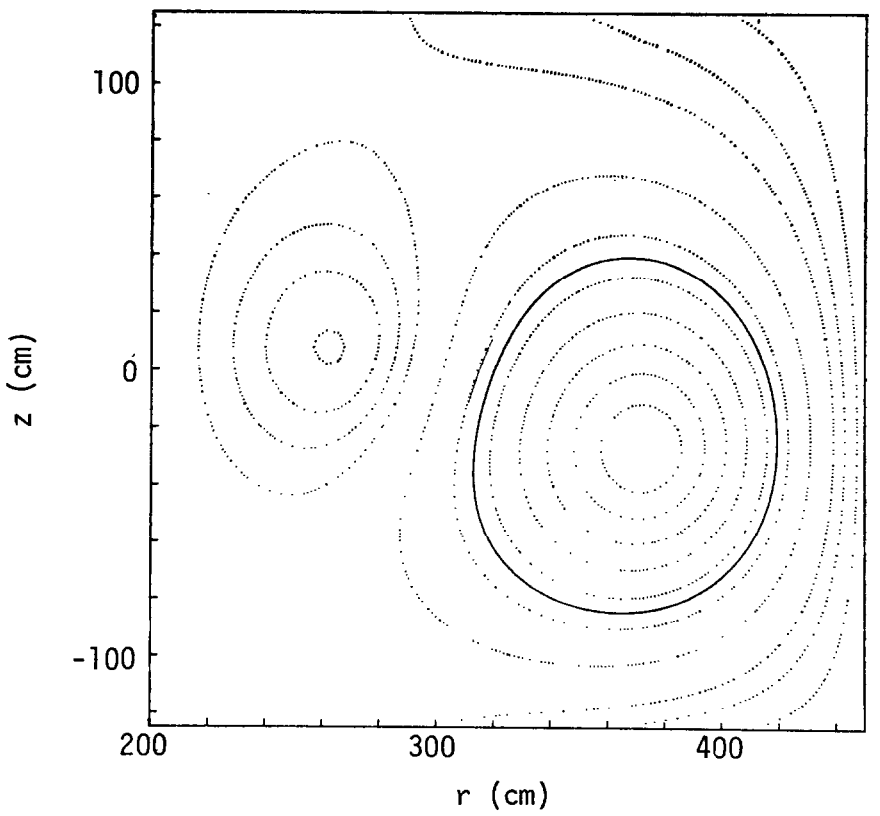

FIG. 8. Poloidal flux surfaces after 75 μsec for co- and counterinjection with $\tau_{inj} = 150$ μsec.

As beam current is injected the poloidal field changes in time and both the plasma equilibrium and the beam particle orbits are affected. It should be noted that the simulated time duration for the computer runs is necessarily much shorter than the beam pulse duration in a realistic experiment. Therefore, in the computer runs we inject the total beam charge, $I_b\tau_b$, in a time τ_{inj} which is short compared to τ_b but still long compared to the drift times for a beam particle.

We present results for three injection conditions: (1) both co- and counterinjected beams are used (one-half of the total beam current in each direction); the beam current buildup time is $\tau_{inj} = 25$ μsec; (2) same as (1), except $\tau_{inj} = 150$ μsec; (3) only coinjection is used, $\tau_{inj} = 150$ μsec.

Results for case (1) after 18 μsec are shown in Figs. 5 and 6. At this time the toroidal particle current flowing in each direction (0.12 MA) is a significant fraction of the bulk plasma current (0.77 MA). In Fig. 5 the two concentrations of particles can be identified with the co- and counterinjected beams, now spatially separated. The corresponding flux plot (Fig. 6) reveals that the plasma has been pushed toward

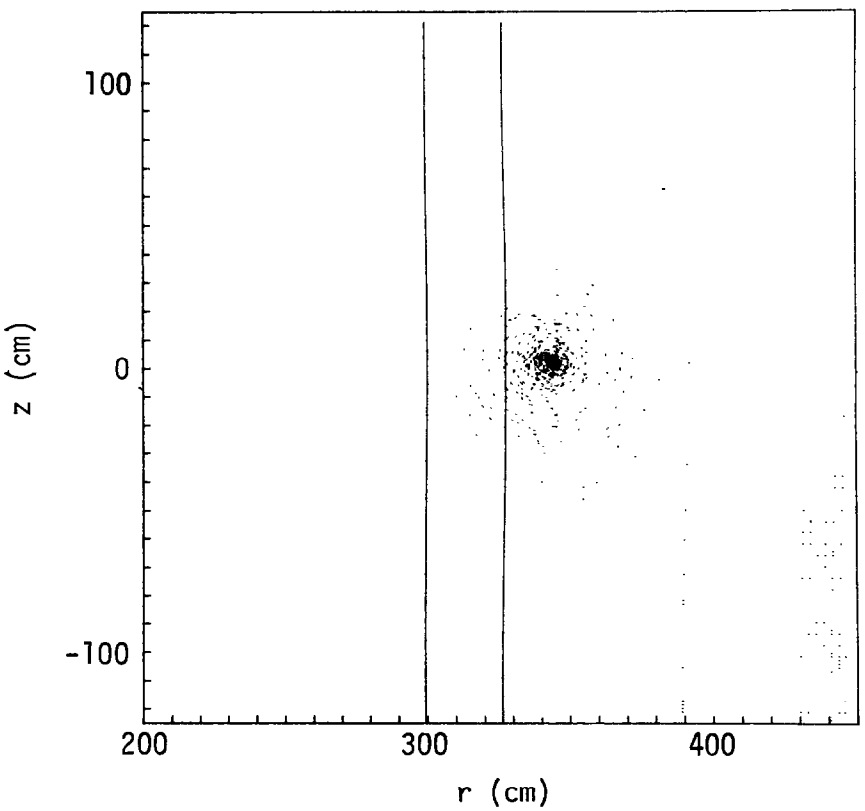

FIG. 9. Particle configuration after 40 μsec for coinjection only with $\tau_{inj} = 150$ μsec.

the edge of the domain and its surface has been deformed. The coinjected and counter-injected currents have repelled one another, while the plasma current and coinjected current have stayed together (parallel currents attract, opposing currents repel). As time proceeds, the gross motion of the system in the (r, z) domain is basically an orbital motion of the oppositely directed currents about one another. The time scale for this orbital motion is observed to be on the order of 1 μsec, in this case.

Results for case (2) after 75 μsec are shown in Figs. 7 and 8. The same mutual repulsion and attraction between current components is obvious, and, in addition, some of the counterinjected particles have had time to drift a considerable distance outside the plasma, where they would normally be lost on a plasma limiter (not included here).

Results for case (3) after 40 μsec are shown in Figs. 9 and 10. To avoid the undesirable distortions associated with counterinjected beams, only coinjection has been used here. No significant change in the distribution of beam particles is observed and the plasma surface, while somewhat expanded, is not distorted. This situation remains unchanged beyond the end of the injection.

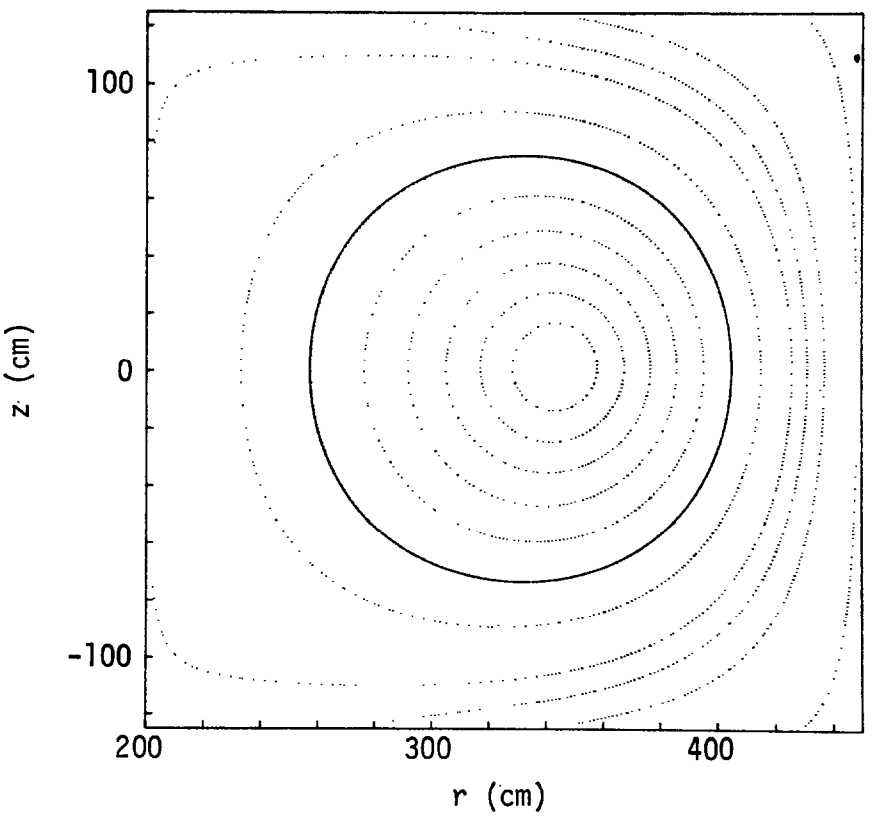

FIG. 10. Poloidal flux surfaces after 40 μsec for coinjection only with $\tau_{inj} = 150$ μsec.

Other variations on these three cases have been investigated and they tend to support the observation presented here that counterinjected beams have a disruptive effect on the equilibrium of the system. Experimental evidence for this behavior in

are:

(1) better treatment of electron plasma currents, including resistivity;

(2) more realistic injection of particles, including spatial and angular distributions;

(3) poloidal beam and plasma currents;

(4) electron drag force on the beam.

Some or all of these refinements may be necessary for a detailed comparison with experiment. Results for the specific application discussed could change as a consequence of these modifications, but the computational model appears to be a workable one.

Appendix

Listed below are the detailed expressions for the three (cylindrical) components of guiding-center velocity (Eqs. (17) and (18)). V is the purely toroidal, externally applied accelerating potential.

$$v_r = v_\parallel \left(\frac{B_r}{B}\right) + \frac{cV}{2\pi}\left(\frac{B_z}{rB^2}\right) - \left(\frac{c}{e}\right)\gamma m_0 v_\parallel{}^2 \frac{1}{B^3}\left(\frac{\partial B_r}{\partial z} - \frac{\partial B_z}{\partial r}\right)\frac{B_r B_\phi}{B}$$
$$+ \left(\frac{c}{e}\right)\left[\frac{\mu}{\gamma} + \frac{v_\parallel{}^2 \gamma m_0}{B}\right]\frac{B_\phi}{B^3}\left(B_r \frac{\partial B_r}{\partial z} + B_z \frac{\partial B_z}{\partial z}\right),$$

$$v_\phi = v_\parallel \left(\frac{B_\phi}{B}\right) + \left(\frac{c}{e}\right)\gamma m_0 v_\parallel{}^2 \frac{1}{B^3}\left(\frac{\partial B_r}{\partial z} - \frac{\partial B_z}{\partial r}\right)\frac{B_r{}^2 + B_z{}^2}{B}$$
$$+ \left(\frac{c}{e}\right)\left[\frac{\mu}{\gamma} + \frac{v_\parallel{}^2 \gamma m_0}{B}\right]\frac{1}{B^3}\left[B_z B_r\left(\frac{\partial B_r}{\partial r} - \frac{\partial B_z}{\partial z}\right) + B_z{}^2 \frac{\partial B_z}{\partial r}\right.$$
$$\left. - B_r{}^2 \frac{\partial B_r}{\partial z} - \frac{B_\phi{}^2}{r} B_z\right],$$

$$v_z = v_\parallel \left(\frac{B_z}{B}\right) - \frac{cV}{2\pi}\left(\frac{B_r}{rB^2}\right) - \left(\frac{c}{e}\right)\gamma m_0 v_\parallel{}^2 \frac{1}{B^3}\left(\frac{\partial B_r}{\partial z} - \frac{\partial B_z}{\partial r}\right)\frac{B_\phi B_z}{B}$$
$$- \left(\frac{c}{e}\right)\left[\frac{\mu}{\gamma} + \frac{v_\parallel{}^2 \gamma m_0}{B}\right]\frac{B_\phi}{B^3}\left(B_r \frac{\partial B_r}{\partial r} + B_z \frac{\partial B_z}{\partial r} - \frac{B_\phi{}^2}{r}\right).$$

ACKNOWLEDGMENT

The authors wish to thank Carol Tull for her assistance in the preparation of the figures for this paper.

REFERENCES

1. S. FISHER AND J. KILLEEN, *Phys. Fluids* **14** (1971), 1240.
2. J. D. CALLEN AND R. A. DORY, *Phys. Fluids* **15** (1972), 1523.
3. D. V. ANDERSON, J. KILLEEN, AND M. E. RENSINK, *Phys. Fluids* **15** (1972), 351.
4. B. MARDER AND H. WEITZNER, *Plasma Phys.* **12** (1970), 435.
5. H. GRAD, *Phys. Fluids* **10** (1967), 137.
6. T. G. NORTHROP, Adiabatic Charged-Particle Motion, *in* "Plasma Physics in Theory and Application" (W. B. Kunkel, Ed.), p. 22, McGraw–Hill, New York, 1966.
7. O. A. ANDERSON AND D. FUSS, *in* "Controlled Thermonuclear Research Annual Report, July 1970–June 1971," pp. 4–9, Lawrence Livermore Laboratory Report UCRL-50000-71.
8. M. BRETTSCHNEIDER, J. KILLEEN, AND A. A. MIRIN, *J. Computational Phys.* **11** (1973), 360.
9. H. L. BERK, H. P. FURTH, D. L. JASSBY, R. M. KULSRUD, T. H. JOHNSON, J. KILLEEN, A. A. MIRIN, M. E. RENSINK, AND C. W. HORTON, JR., *in* "Proceedings of the Fifth Conference on Plasma Physics and Controlled Nuclear Fusion Research, Tokyo, 1974" (IAEA, Vienna, 1975), Vol. III, p. 569.